Characterization of precipitates size distribution: validation of low-voltage STEM

D. ACEVEDO-REYES*†, M. PEREZ*, C. VERDU*, A. BOGNER*
& T. EPICIER*

Université de Lyon, INSA Lyon, MATEIS: UMR CNRS 5510, F69621 Villeurbanne, France

†*CREAS, ASCOMETAL, BP 70045, 57301 Hagondange, France*

Summary

The size distribution of second phase precipitates is frequently determined using conventional transmission electron microscopy (CTEM). However, other techniques, which present different advantages, can also be used for this purpose. In this paper, we focus on high angle annular dark field (HAADF) in TEM and scanning TEM (STEM) in scanning electron microscopy (SEM) imaging modes. The mentioned techniques will be first described, then compared to more conventional ones for the measurement of carbides size distribution in two FeCV and FeCVNb model alloys. This comparative study shows that STEM in SEM, a technique much easier to undertake compared to TEM, is perfectly adapted for size distribution measurements of second phase particles, with sizes ranging between 5 and 200 nm in these systems.

Introduction

Precipitation of second phase particles such as Ti, Nb, and V carbonitrides can have a very positive effect on mechanical properties of microalloyed steels. Low temperature precipitation (in ferrite or in α/γ interphase) leads to a distribution of fine particles, that have a strong strengthening effect (Porter & Easterling 1992). Moreover carbides and carbonitrides stable at high temperature have a pinning effect on austenite grain boundaries (grain size control) leading to optimal mechanical properties (Gladman 2002). For both strengthening and grain size control, it is essential to quantify size distribution and precipitated volume fraction.

Due to the small size of second phase particles (typically a few tenths of nanometers), transmission electron microscopy

(TEM), and particularly conventional TEM (CTEM), appears as one of the most widely used techniques for the characterization and size measurement of precipitates in metal alloys. Among a very large literature concerning this topic, we will concentrate here on methods applied to the case of precipitation within ferrous alloys, which remains of considerable practical and industrial interest, as attested by the following non-exhaustive list of recent examples: precipitation of complex carbonitrides in microalloyed steels (Craven *et al.* 2000; Saikaly *et al.* 2001; Mishra *et al.* 2002), precipitation in a model austenitic steel (Rainforth *et al.* 2002), precipitation of AlN in low carbon steels (Sennour & Esnouf 2003), carbide precipitation in HSLA steels (Hong *et al.* 2003), coherent carbonitride precipitation in commercial microalloyed steels (Morales *et al.* 2003), carbide precipitation at grain-boundaries (Kaneko *et al.* 2004), Nb-based precipitates in ferrite (Beres *et al.* 2004; Perrard *et al.* 2006; Courtois *et al.* 2006).

CTEM on thin foils is well adapted for the observation of carbides (such as VC or NbC) in ferritic steels because the precipitate exhibit the Baker and Nutting (BN) orientation relationship (OR) with the ferritic matrix (Baker & Nutting 1959). In that case, the matrix is simply orientated in a specific crystallographic direction (e.g. ⟨100⟩ ferrite zone axes), and usual dark-field imaging allows to reveal each of the three variants precipitated in the observed area (see for example Perrard *et al.* (2006) in the case of NbC precipitation in low carbon steels). As it will be shown in the present study, CTEM imaging is much less efficient when precipitates do not exhibit any OR with the surrounding matrix.

Recently, new TEM approaches have emerged for the quantitative analysis of precipitation in metal alloys: energy-filtered TEM (EFTEM) and high angle annular dark field (HAADF). These techniques, when applicable, present the advantage to image correctly the precipitates even when no OR exists with respect to the matrix.

EFTEM allows second phases to be imaged in thin foils owing to their difference in chemistry with the matrix. Electrons of the primary beam that have experienced an inelastic scattering caused by a given atomic specie only present in the precipitates can be used to produce an elementary map imaging the particles of interest (Hofer *et al.* 1996; Craven *et al.* 2000; Rainforth *et al.* 2002; Beres *et al.* 2004; Courtois *et al.* 2006; Mackenzie *et al.* 2006) with a very good spatial resolution (i.e. near 1 nm Mackenzie *et al.* (2006)). HAADF in TEM is another imaging method allowing nanometric particles or precipitates to be easily imaged within thin foils and/or when collected on a supporting film (such as extraction replicas in the case of precipitates). In this method, the intensity is roughly proportional to Z^2 (where Z is the atomic number), and excellent contrast is obtained in the case of nanometric particles deposited on holey carbon grids (Treacy & Rice 1989), or carbon or alumina extraction replicas, respectively (Wilson & Craven 2003; Courtois *et al.* 2006). From a practical point of view, extraction replicas represent a very attractive method, when applicable to precipitation problems (see Bradley (1965) and references therein for a general presentation of the replica techniques). After a slight pre-etching, the surface of the material is covered by a nanometric film, and the matrix is further selectively dissolved, allowing precipitates to be retained and observed on the deposited film. In the case of steels, this preparation offers two great advantages: (i) to get rid of the undesirable magnetic influence of the iron matrix during TEM work; and (ii) to allow very large numbers of particles to be measured on a single replica.

Regarding SEM, Varano *et al.* (2005) showed that it is possible to detect niobium carbides using secondary electrons (SE) on replicas in a scanning electron microscope (SEM), but the contrast obtained was not good enough for size distribution measurement. The recent availability of detectors located below the sample allows SEM to produce scanning TEM (STEM) images on thin specimens, which may be of great interest in various situations (Bogner *et al.* 2007). However, to the authors knowledge, STEM in SEM has not been used for the characterization of precipitates in metallic alloys.

In this paper, HAADF in TEM and STEM in SEM imaging techniques will be applied to the particular case of the characterization of carbides size distribution evolution during austenitization of FeCV and FeCVNb model alloys. These techniques will then be compared to more 'conventional' ones, with the aim to validate the STEM approach on replicas in SEM, by comparing it to HAADF in TEM.

Materials and treatments

Model alloys FeCV and FeCVNb

Two high purity model alloys, FeCV and FeCVNb, were used for experimental investigation of the size and composition of vanadium and niobium carbides after different austenitization

Table 1. Compositions of the FeCV and FeCVNb model alloys (in weight %).

	C	V	Nb	S	O	N
FeCV	0.480	0.200	0	<0.0005	<0.0005	<0.0005
FeCVNb	0.470	0.190	0.045	<0.0005	<0.0005	<0.0005

heat treatments. Compositions of these alloys are given in Table 1. Other elements are present in individual quantities less than 5 ppm. Hence, only VC and (V,Nb)C carbides are expected to precipitate.

Plates of these model alloys were manufactured by the PECM group at the ENSM., Saint Etienne, France. The final thickness of the plates was about 2 mm. The last stage of the elaboration process was a solutionizing heat treatment at 1000°C for 30 min followed by a water quench to room temperature (Fig. 1). Samples of 70 mm × 5 mm × 1 mm were taken from the core region of the plates to avoid the decarburized zone at their periphery. All different heat treatments described later were performed on these samples.

Heat treatments

A two-step heat treatment was designed to precipitate almost all the vanadium and the niobium of the alloy with a high volume fraction of precipitates, and to obtain precipitate sizes as large as possible. In the first step, they were further heated at 700°C for 10 h in vacuum (quartz encapsulation). In the second step, samples were then heated at 800°C for 10 days (to allow coarsening in austenite), and finally slowly cooled down to room temperature (Fig. 1). The pertinence of this two-step procedure is detailed elsewhere (Epicier *et al.* 2008). This state (called fully precipitated state [FPS]), was chosen as the starting point for a series of isothermal heat treatments in austenite. In order to validate the STEM approach on replicas on different precipitation states, FPS samples were heat treated at different temperatures between 870 and 1200°C, and for different holding times from 2 min to 9 days. These reversion experiments were performed either in a molten salt bath or in a furnace under quartz encapsulation. Samples were water quenched to room temperature. The obtained states will be hereafter called as partially dissolved states (PDS) (Fig. 1).

Experimental techniques and procedures

Microscopy work

SEM and CTEM techniques are widely known and will not be detailed in this paper. It can just be noted that the introduction of field emission gun (FEG) in SEM allows a resolution of about 2 nm in the secondary electrons (SE) imaging mode.

SEM was performed with a FEG SEM (XL30 from FEI) (FEI, Hillsboro, OR) operating at 30 kV. SE imaging was done using
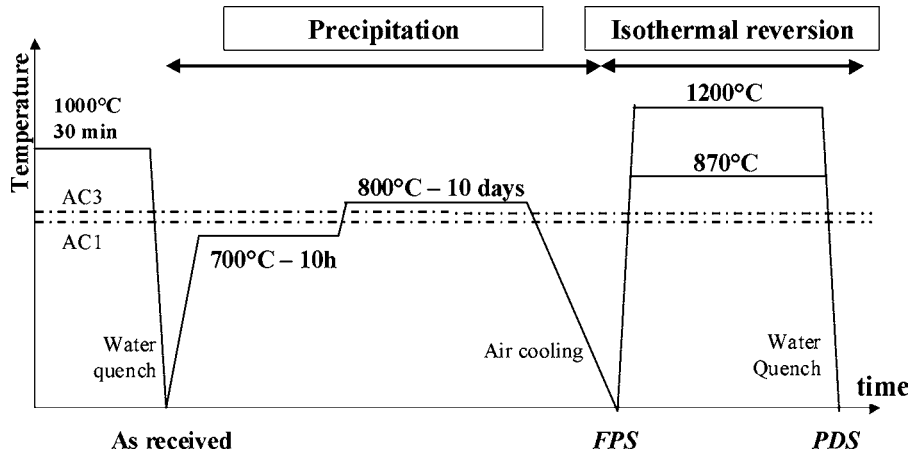
Fig. 1. Heat treatments performed on FeCV and FeCVNb samples.

an Everhart-Thornley detector, whereas STEM imaging in this SEM microscope was done using a STEM detector. In order to check the nature of precipitates (i.e. presence of V or Nb), chemical analysis has been conducted using an analysing system from EDAX (EDAX, Mahwah, NJ).

CTEM imaging was performed using a 2010F microscope from JEOL (JEOL, Tokyo, Japan). Precipitates were examined using conventional imaging techniques, electron diffraction and EDX with an OXFORD-Inca analyser (OXFORD, Abington, U.K.) used to confirm the chemistry of precipitates. Further HAADF imaging was performed using a JEOL annular detector. This detector is placed well under the projecting lenses below the sample, and collects only incoherent electrons scattered at angles much higher than Bragg's angles. According to Rutherford scattering, the intensity at each probe position is given by:

$$I = C \sum n_i Z_i^2, \qquad (1)$$

where n_i is the number of atoms with atomic numbers Z_i in the irradiated volume, C a constant of proportionality (taken equal to unity in the following for sake of simplicity).

Because of the difference in atomic number between niobium or vanadium and carbon (respectively 41 and 23 against 6), this technique is very efficient to image vanadium or niobium carbides on carbon extraction replicas with a good contrast. Furthermore, it is particularly adapted to obtain easily size distributions because of the large number of particles that can be observed in a reasonably short time, and easily analysed with semi-automatic image treatments, owing to their high contrast.

As permitted by the XL30 SEM, STEM imaging was also tested by using a solid-state detector placed below the sample in the microscope (Fig. 2). Its dipolar constitution allows 'bright-field' or 'dark-field' images to be acquired by choosing one of the two diodes (i.e. by collecting either preferentially transmitted or deflected electrons over an angular range of several degrees). In this work, only 'dark-field' imaging has been performed.
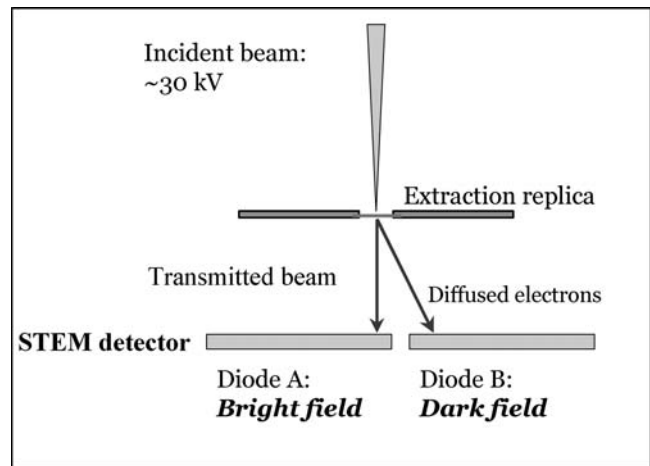

Fig. 2. STEM detector in SEM: a BSE detector is positioned below the sample.

The intensity of these images depends in a complex way on the chemical composition, because deflected electrons have experienced different interaction mechanisms (elastic or inelastic scattering). Hence, it is difficult to establish a direct link between the intensity of the particles and their chemical composition as permitted in HAADF on the basis of Eq. 1. According to Fig. 2, the collection conditions cannot be strictly controlled as in the case of an annular detector. Nevertheless, detection angles estimated in our case are ranging from 10 to a few dozens degrees in a limited angular sector. As it will be observed in the following, resulting images exhibit satisfying contrast.

Sample preparation

For conventional SEM observations of bulk samples, their surface was polished to 1/4 mm diamond paste, and then chemical etched with an 0.4% nital solution. Transmission electron microscopy studies were carried out on both thin

Table 2. Summary of performed experiments for testing (T) or measurements (M). STEM imaging on bulk samples in SEM (shaded box) is not possible for obvious reasons. (*) In this table thin foils are considered as "bulk" as precipitates are embedded in iron matrix.

technique / sample	SEM		TEM	
	SE	STEM	CTEM	HAADF-STEM
bulk*	M		M	T
Extraction replicas	T	M	T	M

foils and carbon extraction replicas. Thin foils were prepared by mechanical polishing to a final thickness of 20–30 μm (in order to minimise the undesirable magnetic effects during observation), followed by an argon ion beam thinning process in a polishing precision system (PIPS) from GATAN (GATAN, Pleasantown, CA). Carbon extraction replicas were prepared following a standard procedure: samples were first polished and etched in 0.4% nital. The etched surface was then coated with a thin film of carbon ($\approx$20 nm) and then scored into 2-mm squares. Finally, samples were etched in diluted nital to remove the thin film from the substrate. The extracted carbon replicas were then rinsed in both ethanol and methanol, placed on copper grids and dried.

Comparative study of CTEM, SE in SEM, HAADF in TEM and STEM in SEM

Summary of results

As discussed above, different combinations of imaging techniques and sample nature are possible, and were tried as summarized in Table 2.

In order to compare these different approaches, the FPS of the FeCV alloy has been investigated using SE in SEM on bulk samples, CTEM on thin foils, HAADF in TEM on carbon replicas and STEM in SEM on carbon replicas. As pointed out in Table 2, the remaining possibilities were only briefly tested for reasons developed in the next sub-sections. Figure 3
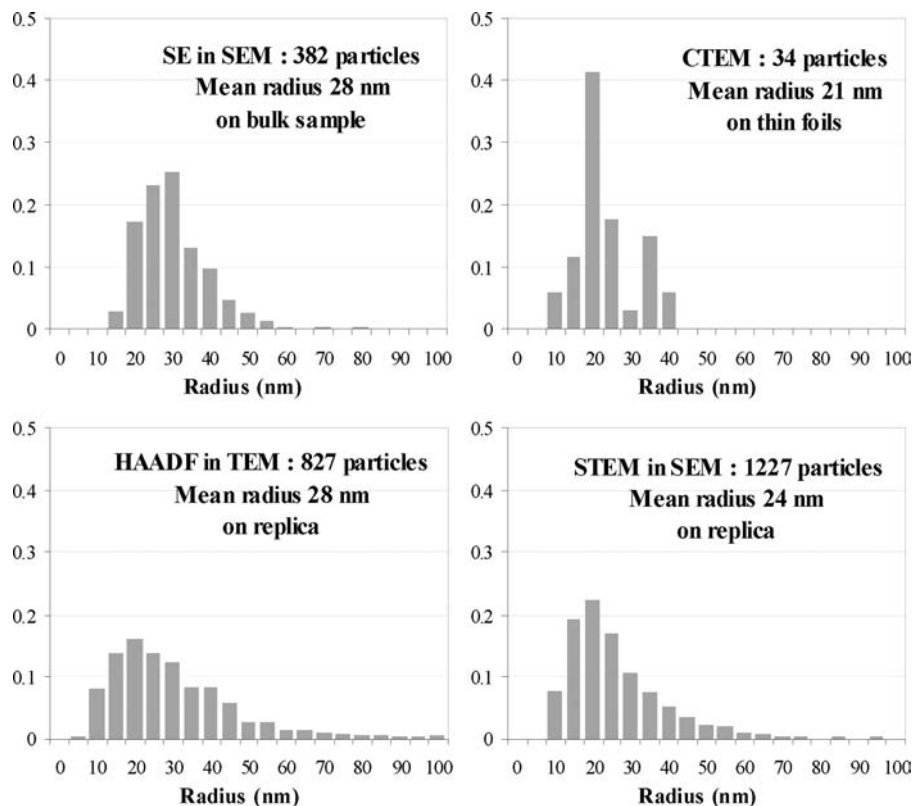

Fig. 3. Particle size distribution of the FPS of the FeCV alloy measured by different techniques: CTEM, SE in SEM, HAADF in TEM and STEM in SEM. The vertical scale is the precipitation density. It can be seen that the four techniques give comparable results.
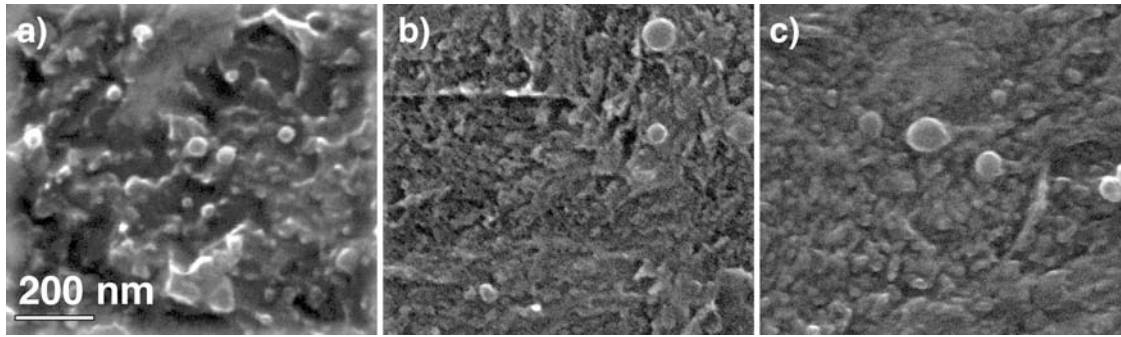
Fig. 4. SEM micrographs of the FeCV alloy at high magnification showing vanadium carbide particles for different states : (a) fully Precipitated State (FPS), (b) 870°C 2 min; (c) 920°C 60 min.

shows the particles size distributions obtained in each case, the number of measured particles, and the calculated mean radius are also indicated. Representative micrographs obtained with these four approaches will be reported in the following.

The shape of the size distribution and the value of the mean radius obtained with the four different techniques are very similar (Fig. 3), and thus, they all seem to be adapted for size measurements of second phase particles such and drawbacks in each case in terms of rapidity, efficiency and facility.

SEM in SE mode

Figure 4 shows three micrographs of different precipitation states obtained on bulk specimen with the SEM in SE mode. Although precipitates are visible, their contrast is not sufficient for automatic image analysis. Furthermore, particles seem to be covered by a remaining layer of iron probably, leading to difficulties in clearly identifying their contour. Although particle size distributions can readily be obtained with this technique, for example see Acevedo-Reyes *et al.* (2005), the number of particles that can be unambiguously and accurately measured from such images in a reasonable time appears to be too low in order to obtain statistically representative results (about a hundred during a half-day observation).

Conventional TEM on thin foils

In the particular case of the present investigation, it must be recalled that carbides have lost any orientation relationship with the matrix following the ferrite to austenite phase transformation during the precipitation heat treatment. Hence, it is not possible to use the conventional dark field (DF) mode to observe easily numerous particles in the same precipitation variant.

However, as shown in Fig. 5, particles are easily visible in bright field images, but their contrast is not sufficient for an automatic image analysis. Precipitates observed in bright field can look either bright or dark, depending on diffraction conditions. Combining the fact that (i) particles do not have

any OR with the matrix, (ii) martensite is magnetic, and (iii) the area analysed in a thin foil is quite small, the number of particles that can be observed in a reasonable time is very low (2 or 3 dozens during a half-day observation). Consequently, TEM on thin foils is not adapted for determining the size distribution in the present case.

HAADF-STEM on thin foils in TEM

As reported in Table 2, HAADF imaging on thin foils in a TEM was only performed for testing purposes (see Fig. 6). Contrary to the case of supported carbides on extraction replicas, vanadium or niobium carbides exhibit poor contrasts in HAADF images from iron thin foils. Equation 1 can be used to predict the contrast of VC and NbC particles, considered as perfect spheres, embedded in a thin foil of iron with a given thickness. Neglecting beam spreading (i.e. assuming a constant probe size throughout the sample), and taking into account atomic densities in numbers of atoms per unit volume,[1] elementary HAADF intensities per nm^3 can be calculated as

$$\begin{aligned} I_{Fe} &= 57460, \\ I_{VC} &= 31188 \text{ and} \qquad (2) \\ I_{NbC} &= 76922. \end{aligned}$$

A simple computation of the precipitate geometry allows HAADF micrographs to be simulated. Figure 6(a) is a conventional bright field image of two precipitates, with a similar size ϕ of about 60 nm, in a FeCVNb alloy. EDX analysis (not shown here for the sake of brevity) indicates that the particle on the left is vanadium-rich, whereas the one on the right is Nb-rich. In the HAADF image (Fig. 6(b)), the VC precipitate surprisingly vanishes. A careful examination of expressions 1 and 2 implies that this experimental result can only be explained if the matrix thickness t (which enters

1. $\rho_{Fe} = 85.0 \, nm^{-3}$ (describing the iron matrix as pure ferrite, with $a = 0.2866$ nm), $\rho_{V \, in \, VC} = \rho_{C \, in \, VC} = 55.2 \, nm^{-3}$ (with fcc VC, with $a = 0.417$ nm) and $\rho_{Nb \, in \, NbC} = \rho_{C \, in \, NbC} = 44.8 \, nm^{-3}$ (with fcc NbC, with $a = 0.447$ nm).
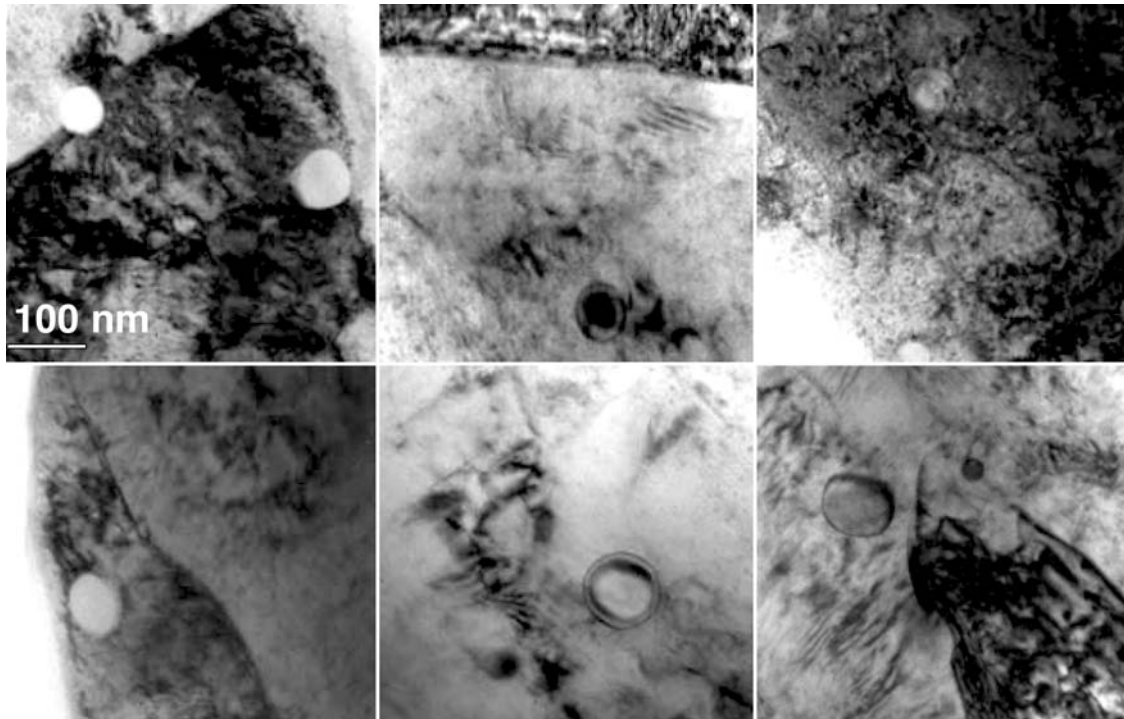
Fig. 5. Bright Field TEM micrographs of different reversion states of the FeCV alloy. In some cases the contrast between precipitates and matrix is poor due to the diffraction conditions.

into the expression of the number of irradiated atoms n_i of Eq. 1) is smaller than the precipitate size, and if the particles are not totally embedded into the matrix. Computations performed varying (i) the matrix thickness; (ii) the precipitates embedding depth within matrix lead to the reasonable configuration as shown in Fig. 6(c), where each precipitate is only partly buried on 30 nm within a 50-nm iron matrix. Simulated images confirm that the vanadium carbide particle cannot be discerned under those HAADF conditions (the difference in intensity between the VC particle and the surrounding Fe matrix, hardly discernable on the simulation, is about 4%).

According to this, HAADF imaging of iron thin foils does not appear to be well adapted to the identification of carbides in the present case.

CTEM observations on carbon extraction replica

In order to avoid the magnetism of the matrix and to analyse a large number of particles, observations can be carried out on carbon extraction replica. For clarity of the comparison between the different observation modes applicable to carbon extraction replicas, Figure 7 reports a montage of micrographs
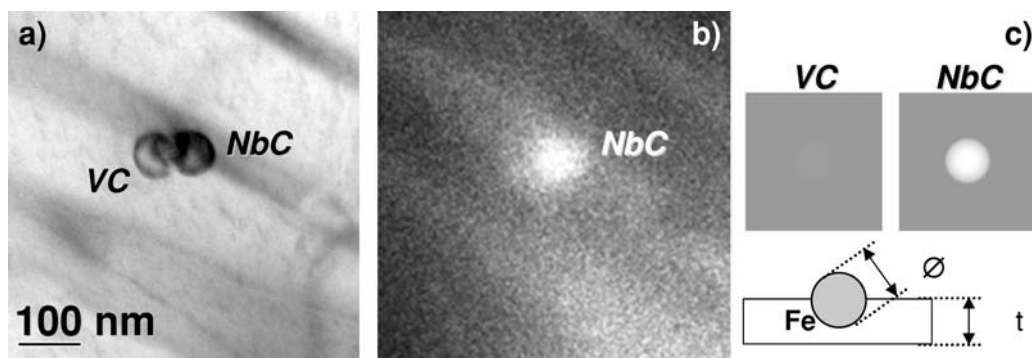

Fig. 6. HAADF imaging of precipitates in the FeCVNb model alloy (FPS state): (a) conventional bright field image showing two precipitates in a perlite grain; (b) corresponding HAADF image; (c) simulations of HAADF images for pure VC and NbC particles according to the geometry sketched below (see text for details).
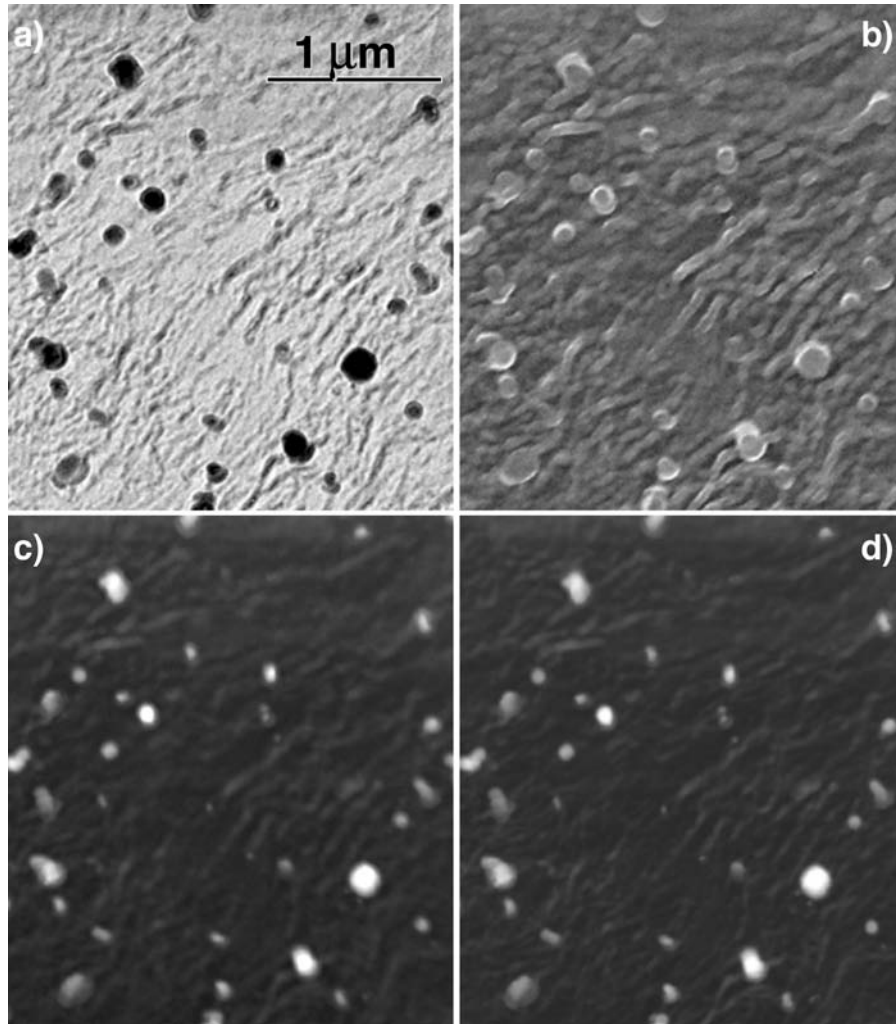
Fig. 7. Micrographs of the same area of a carbon extraction replica of the FeCV alloy obtained by different imaging modes: (a) CTEM, (b) SE in SEM, (c) HAADF, (d) STEM in SEM; all carried on carbon extraction replica of the sample heat treated 2 min at 870°C.

from the same area imaged with different techniques. Figure 7(a) is a CTEM image of such a replica. Particles are clearly observed and their size can be measured easily. The main limitation arises from diffraction conditions, which makes that some particles exhibit a contrast very close to that of the supporting carbon film. Hence, some precipitates are difficult to identify and measure accurately. By comparison, STEM images (Fig. 7(c–d) exhibit stronger contrast and will thus be preferred for a statistical analysis of particles.

HAADF imaging of carbon extraction replica

Figure 7(c) shows an HAADF micrograph of the same area than previously imaged in CTEM. The high number of particles observed and the high contrast obtained allows an automatic image analysis for the determination of the particle size distribution. Considering relations 1 and 2, and according to the basic development proposed in section 'HAADF-STEM on

Thin Foils in TEM', a quantitative analysis of HAADF images is possible in order to relate intensities to the chemistry (V-rich or Nb-rich in the case of the FeCVNb alloy) of particles (work in progress).

SEM Observations on replicas: SE mode

From the above, it is clear that the particle size distribution can be easily measured by TEM in HAADF. However, a motivation of this study is to check whether such measurements can also be efficiently performed with a SEM, because the latter instrument is more accessible and easier to use especially for the industry.

Figure 7(b) shows a micrograph of the same zone as previously described, obtained in a SEM in SE mode. Particles are clearly discernable, but again the contrast obtained is not high enough for allowing an automatic image analysis.
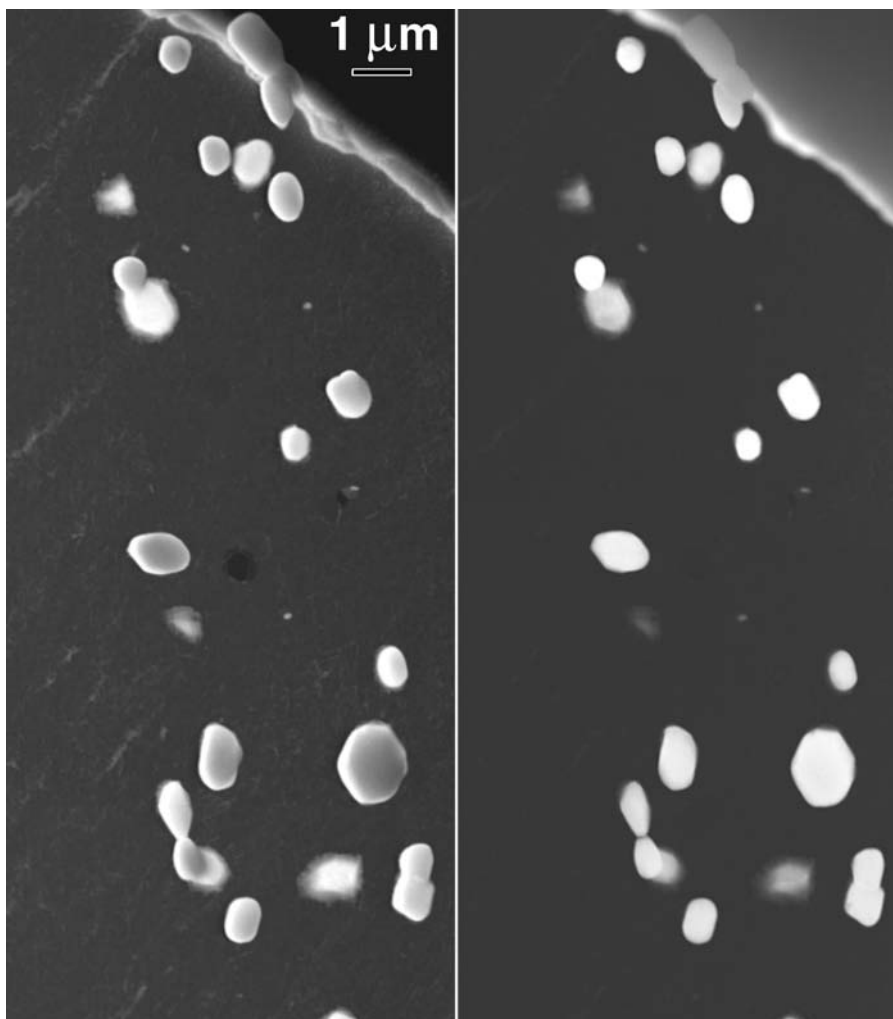
Fig. 8. Micrographs on carbon extraction replica of FeCVNb after 5 days at 1200°C: (a) HAADF in TEM, (b) STEM in SEM. Note that the HAADF image seems to be more contrasted because of the larger dynamic of the 16 bits recorded images which is considerably reduced in a 8 bits grey level display.

SEM Observations on replicas: STEM mode

Finally, Figure 7(d) shows the STEM micrograph of the same area observed in the SE-SEM and TEM modes. It can be noticed that the contrast is very good, which is favourable for a quantitative analysis of the precipitates. Furthermore, the image is spectacularly similar to that obtained in HAADF: only very subtle differences can be observed in the contrast of the particles or in the contrast of the replica.

The degree of resemblance between STEM-SEM and HAADF-TEM images is however directly influenced by the size and the chemistry of the particles. Figure 8(a,b) compares HAADF-TEM and STEM-SEM micrographs of extraction replica from the FeCVNb alloy austenitized at 1200°C for 5 days. The particles observed in this state are significantly larger and 'heavier' (owing to the presence of niobium) than the particles showed in Fig. 7. Once again, both imaging techniques show the same size of particles, but there are now obvious differences in their contrast. According to relation 1, the HAADF intensity is a monotone function of the composition and the thickness of the particles; hence, if the particles have the same chemical composition, the bigger they are, the whiter they appear. In SEM, the contrast of the biggest particles is here different: they appear dark in the centre. This inversion of contrast is partly due to the energy of the incident beam: in TEM, incident electrons have a sufficient energy (200 kV) to pass across the largest particles without any significant losses which would decrease the scattered intensity collected by the annular detector, whereas 30 kV electrons in the SEM experience efficient back-scattering or other inelastic processes for larger particles which decrease the collectable STEM signal compared to thinner particles. Furthermore, other parameters, such as the detector geometry and the range of collection angles, might also affect the STEM contrast in the SEM.
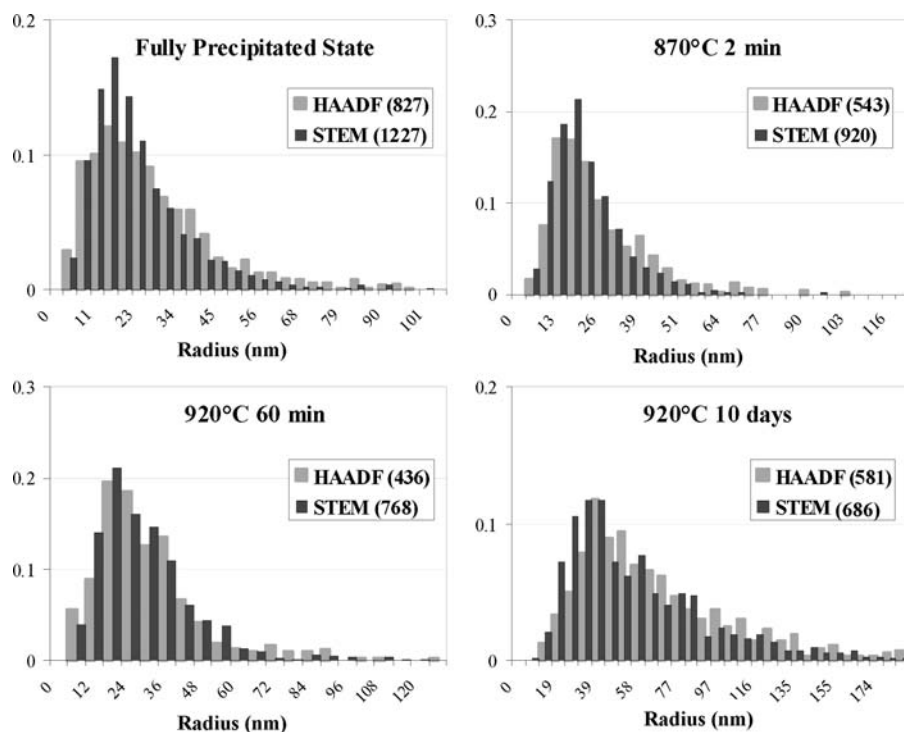
Fig. 9. Particle size distributions obtained on different states of the FeCV alloy. In each case, the results obtained in STEM in SEM are compared to the results obtained in HAADF in TEM. The number of particles measured appears in parenthesis.

Validation of STEM in SEM

It has been shown that the STEM imaging mode in the SEM leads to micrographs with a contrast adapted for the particle size distribution determination. However, to the authors' knowledge, this technique has not been used for this purpose, and must be validated. Hence, particle size distributions obtained with this technique were compared with particle size distributions obtained from HAADF images (Fig. 5). It should be noticed here that the observed areas with both techniques were chosen randomly.

Particles were identified and measured by a semi-automatic image analysis. The error due to the fact that measurements were made on projections is negligible because the particles observed are spherical in most of the cases (only after long heat treatments, e.g. 1200°C 5 days for example, particles tend to lose their sphericity).

Figure 9 shows the particle size distributions of four different states of the FeCV alloy. To make the comparison easier between results obtained in STEM and in TEM, normalized densities of distribution have been represented. The results obtained with both techniques are in good agreement. Even when the shape of the distribution is slightly different, the maximum of the density appears for the same radius range. Furthermore, the mean radius values calculated from the particle size distributions obtained with both techniques are very similar, and the maximal difference observed in the case of the FeCV

alloy is less than 20%. Observations performed on the same zone (Fig. 8; STEM in SEM and HAADF in TEM) lead to a difference of 4% in mean radius. As the measurements were done on different replicas and that the number of particles observed is not always the same, we can conclude that both techniques give the same result.

STEM imaging mode on SEM is thus an efficient way for the determination of carbide size distributions in the present case. However, two limitations remain: (i) the resolution is limited by the SEM probe size (in our case precipitates as small as 5 nm have been imaged); (ii) in our configuration, the chemistry of the particles cannot be ascertained by a quantitative contrast analysis (as it should be possible in the TEM HAADF mode) because of the non-annular geometry of the STEM detector.

Note that although improved by the use of thin specimens, EDX chemistry analysis in SEM is not applicable to the smallest particles. TEM is thus required when it is necessary to determine the chemical nature of the particles, such as in the case of the FeCVNb alloy where it is interesting to separate the populations of V-rich, Nb-rich or rather mixed V-Nb carbides (Perez *et al.* 2008).

Nevertheless, the interest of the STEM imaging technique in SEM can be illustrated in the case of the study of particle size evolution during isothermal reversion of FeCV alloy. Figure 10 presents the evolution of the mean radius at three temperatures: 870, 920, and 950°C. It should be
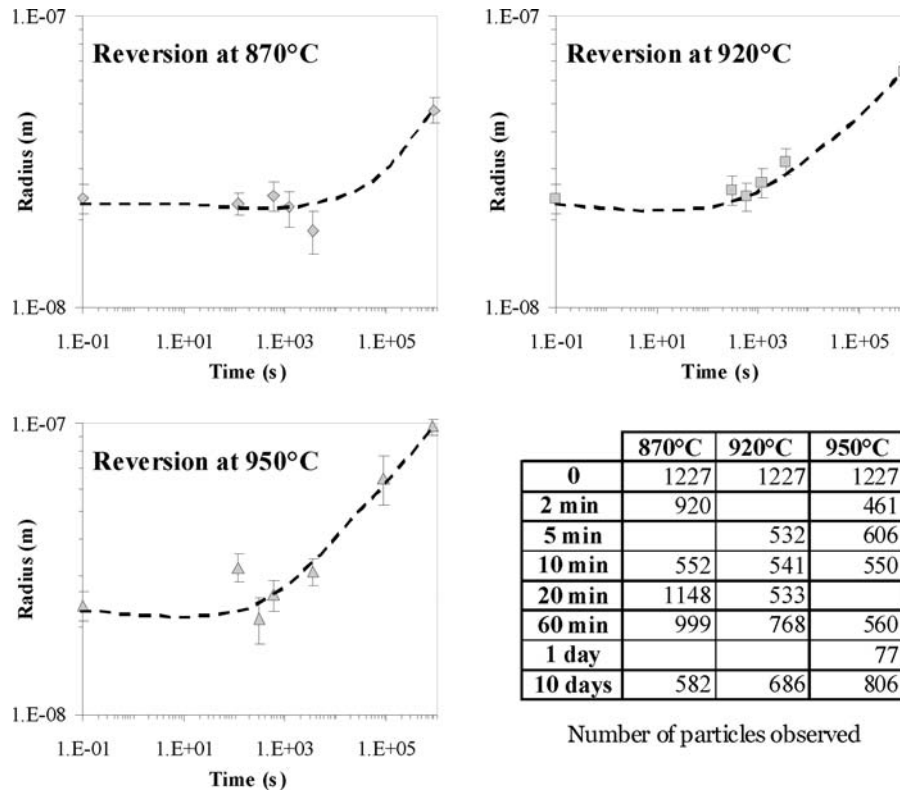
	870°C	920°C	950°C
0	1227	1227	1227
2 min	920		461
5 min		532	606
10 min	552	541	550
20 min	1148	533	
60 min	999	768	560
1 day			77
10 days	582	686	806

Number of particles observed

Fig. 10. Mean radius evolution during isothermal reversion of FeCV alloy at three different temperatures : 870, 920 and 950°C.

emphasized that the numbers of experimental measurements are reasonably representative from a statistical point of view, which permits for example to use these data to calibrate a model of precipitation and dissolution kinetics of VC as presented elsewhere (Acevedo *et al.* 2008).

Conclusions

The aim of this paper was to compare different imaging techniques for the determination of particles size distributions in both FeCV and FeCVNb alloy. Main conclusions can be summarized as follows:

1. As a general trend, SEM and TEM imaging techniques on both bulk samples and carbon extraction replica can give comparable particle size measurements, but time considerations reduce the interest of observations on bulk samples (SE in SEM and CTEM or HAADF on thin foils), because it may be extremely tedious to collect sufficiently large number of data in order to obtain representative results.
2. Particles size distributions can be perfectly determined in SEM when extraction replicas are feasible.
3. Observations on carbon replica, both in HAADF imaging technique and STEM mode in SEM, allow large populations of particles to be measured in a semi-automatic way owing to the high contrast of micrographs.
4. STEM in SEM was validated for the particle size measurement by comparing it to the HAADF imaging technique.
5. However, the use of STEM in SEM is restricted to the cases where the knowledge of the particles chemistry is not required, according to the fact that very small precipitates can be difficult to analyse confidently in SEM by EDX. In such cases, HAADF-TEM will be preferred.
6. STEM in SEM technique was successfully used to follow the evolution of the populations of VC particles during austenitization of a FeCV alloy at different temperatures.

Acknowledgements

References

Acevedo, D. Evolutions de l'etat de precipitation au cours de l'austénitisation d'aciers microalliés au vanadium et au niobium. PhD Thesis, INSA de Lyan. (available online).

Acevedo, D., Perez, M., Epicier, T., Kozeschnik, E., Perrard, F. & Sourmail, T. (2008) Kinetics of precipitation and dissolution in model FeCV and FeCVNb alloy, and a microalloyed ultra high strength spring steel. In *New Developments on Metallurgy and Applications on High Strengh Steels*. TMS, Conference 2008.

Acevedo-Reyes, D., Perez, M., Pecoraro, S., Vincent, A., Epicier, T. & Dierickx, P. (2005) Vanadium carbide dissolution during austenitisation of a model microalloyed fecv steel. *Mat. Sci. Forum* **500–501**, 695–702.

Baker, R.G. & Nutting, J. (1959) The tempering of a Cr-Mo-V-W and a Mo-V steel. In *Precipitation processes in steels*, pp. 1–22. Iron and steel institute, London.

Beres, M., Weirich, T.E., Hulka, T.E. & Mayer, J. (2004) TEM investigations of fine niobium precipitates in HSLA steel. *Steel Res. Int.* **75**, 753–758.

Bogner, A., Jouneau, P.H., Thollet, G., Basset, D. & Gauthier, C. (2007) A history of scanning electron microscopy developments: towards wet-STEM imaging. *Micron* **38**, 390–401.

Bradley, D.E. (1965) Replica and shadowing techniques. In *Techniques for Electron Microscopy*, pp. 96–165. Blackwell, Oxford.

Courtois, E., Epicier, T. & Scott, C. (2006) EELS study of niobium carbonitride nano-precipitates in ferrite. *Micron* **37**, 492–502.

Craven, A.J., He, K., Garvie, A.J. & Baker, T.N. (2000) Complex heterogeneous precipitation in titanium niobium microalloyed Al-killed HSLA steels I&II. *Acta Mater.* **48**, 3857–3878.

Epicier, T., Acevedo, D. & Perez, M. (2008) Crystallographic structure of vanadium carbide precipitates in a model Fe-C-V steel. *Phil. Mag.* **88**, 31–45.

Gladman, T. (2002) *The Physical Metallurgy of Microalloyed Steels*. The Institute of Materials, London.

Hofer, F., Warbichler, P., Buchmayr, B. & Kleber, S. (1996) On the detection of MX-precipitates in microalloying steels using EFTEM. *J. Microsc.* **184–3**, 163–174.

Hong, S.G., Kang, H.J. & Park, C.G. (2003) Evolution of precipitates in the Nb-Ti-V microalloyed HSLA steels during reheating. *Scripta Mater.* **48**, 1201–1206.

Kaneko, K., Matsumura, S., Sadakata, A., Fujita, K., Moon, W.J., Ozaki, S. & Tomokiyo, N. (2004) Characterization of carbides at different boundaries of 9Cr-steel. *Mater. Sci. Eng.* **A374**, 82–89.

Mackenzie, M., Craven, A.J. & Collins, C.L. (2006) Nanoanalysis of very fine VN precipitates in steel. *Scripta Mater.* **54**, 1–5.

Mishra, S.K., Das, S. & Ranganathan, S. (2002) Precipitation in hight strength low alloy (HSLA) steel: a TEM study. *Mater. Sci. Eng.* **A323**, 285–292.

Morales, E.V., Gallefo, J. & Kestenbach, H.J. (2003) On coherent carbonitride precipitation in commercial microalloyed steels. *Phil. Mag. Lett.* **83**, 79–87.

Perez, M., Dumont, M. & Acevedo, D. (2008) Implementation of the classical nucleation theory for precipitation. *Acta Mater.*, **56**, 2119–2132.

Perrard, F., Donnadieu, P., Deschamps, A. & Barges, P. (2006) TEM study of NbC heterogeneous precipitation in ferrite. *Phil. Mag.* **86**, 4271–4284.

Porter, D.A. & Easterling, K.E. (1992) *Phase transformation in metals and alloys*. Chapman and Hall, London. 514p.

Rainforth, W.M., Black, M.P., Higginson, R.L., Palmiere, E.J., Sellars, C.M., Prabst, I., Warbichler, P. & Hofer, F. (2002) Precipitation in a model austenitic steel. *Acta Mater.* **50**, 735–747.

Saikaly, W., Bano, X., Issartel, C., Rigault, G., Charrin, L. & Charai, A. (2001) The effects of thermomechanical processing on the precipitation in an industrial dual-phase steel microalloyed with Titanium. *Metall. Mater Trans.* **A32**, 1939–1947.

Sennour, M. & Esnouf, C. (2003) Contribution of advanced microscopy techniques to nano-precipitates characterization: case of AlN precipitation in low-carbon steel. *Acta Mater.* **51**, 943–957.

Treacy, M. M.J. & Rice, S.B. (1989) Catalyst particle sizes from rutherford scattered intensities. *J. Microsc.* **156**, 211–234.

Varano, R., Elwazri, A.M., Siciliano, F., Bai, R., Gauvin, R. & Yue, S. (2005) FE-SEM study of fine nb precipitates in carbon extraction replicas. *Mater. Sci. Forum* **500–501**, 663–668.

Wilson, J.A. & Craven, A.J. (2003) Improving the analysis of small precipitates in HSLA steels using a plasma cleaner and ELNES. *Ultramicroscopy* **94**, 197–207.